Volume 12
Number 35
21 September 2021
Pages 11607–11924

Chemical Science

rsc.li/chemical-science

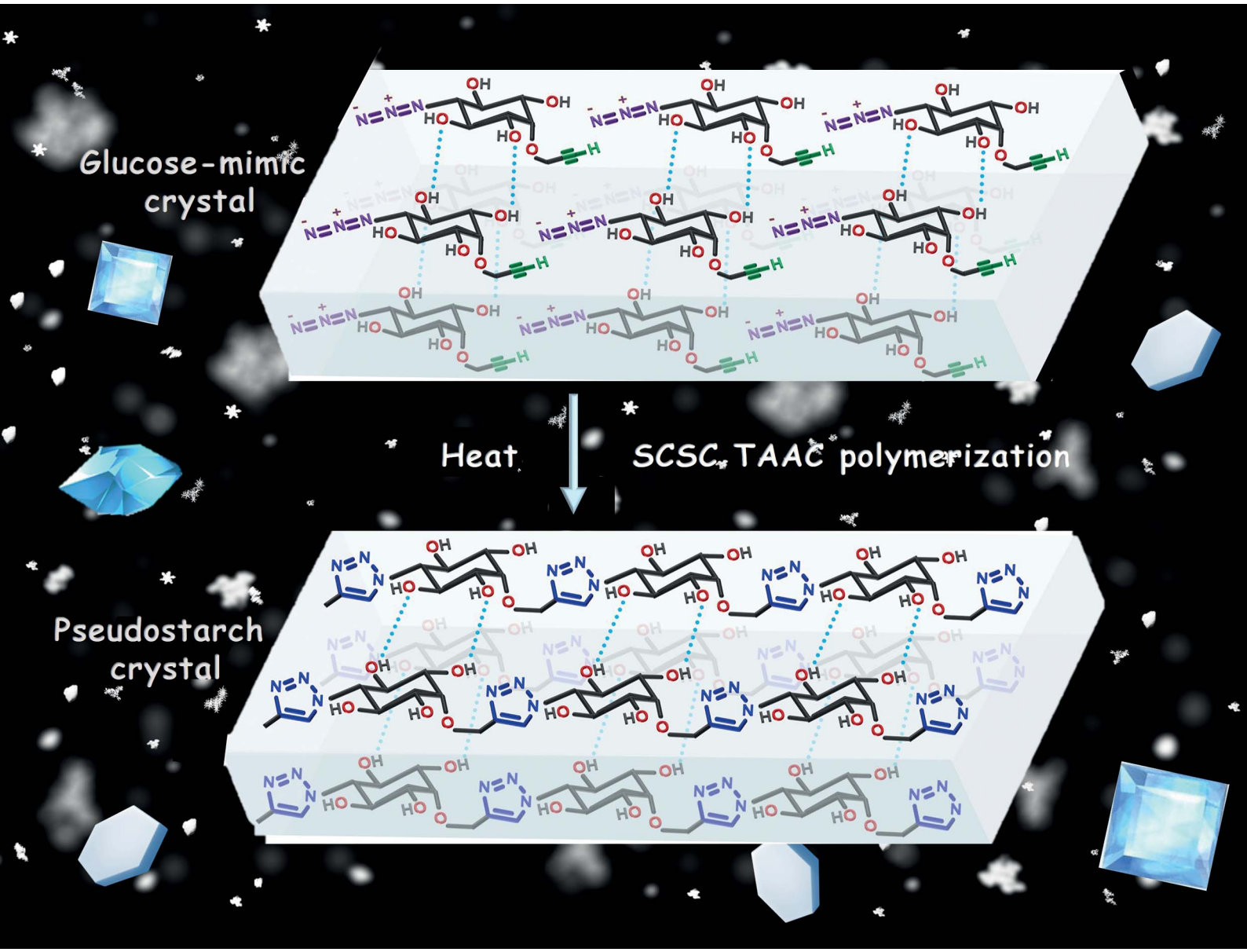

ISSN 2041-6539

ROYAL SOCIETY OF CHEMISTRY

EDGE ARTICLE
Kana M. Sureshan *et al.*
Single-crystal-to-single-crystal synthesis of a pseudostarch *via* topochemical azide–alkyne cycloaddition polymerization

Chemical Science

ROYAL SOCIETY OF CHEMISTRY

EDGE ARTICLE

Cite this: *Chem. Sci.*, 2021, **12**, 11652

All publication charges for this article have been paid for by the Royal Society of Chemistry

Received 8th July 2021
Accepted 5th August 2021

DOI: 10.1039/d1sc03727g

rsc.li/chemical-science

Single-crystal-to-single-crystal synthesis of a pseudostarch *via* topochemical azide–alkyne cycloaddition polymerization†

Arthi Ravi, Amina Shijad and Kana M. Sureshan *

There is high demand for polysaccharide-mimics as enzyme-stable substitutes for polysaccharides for various applications. Circumventing the problems associated with the solution-phase synthesis of such polymers, we report here the synthesis of a crystalline polysaccharide-mimic by topochemical polymerization. By crystal engineering, we designed a topochemically reactive crystal of a glucose-mimicking monomer decorated with azide and alkyne units. In the crystal, the monomers arrange in head-to-tail fashion with their azide and alkyne groups in a ready-to-react antiparallel geometry, suitable for their topochemical azide–alkyne cycloaddition (TAAC) reaction. On heating the crystals, these pre-organized monomer molecules undergo regiospecific TAAC polymerization, yielding 1,4-triazolyl-linked pseudopolysaccharide (pseudostarch) in a single-crystal-to-single-crystal manner. This crystalline pseudostarch shows better thermal stability than its amorphous form and many natural polysaccharides.

Introduction

There is a growing interest in synthesizing polymers modeled after natural polysaccharides in view of their improved properties, enzymatic stability, *etc.*1 Syntheses of several pseudopolysaccharides containing monosaccharide units or their mimics connected by unnatural linkages have been achieved.[1b,2] Inositols (hexahydroxy cyclohexanes),[3] being structural mimics of hexose sugars, are attractive monomers for the synthesis of pseudopolysaccharides.[4] However, unlike monosaccharides, which can homopolymerize in view of their electrophilic (carbonyl) and nucleophilic (hydroxyl groups) functionalities, inositols do not have such complementary reactive groups and require an external linker to form polymers. The 1,2,3-triazole unit is a robust, unnatural linker that confers many attractive properties to polymers.[5] The use of conventional solution-phase synthesis of triazoles for polymer synthesis is limited due to the difficult purification of the polymer from catalysts, reagents and side products.[6,7] Circumventing these issues, here we report the uncatalyzed, regiospecific single-crystal-to-single-crystal (SCSC) synthesis of a starch-like pseudopolysaccharide (Fig. 1) from *myo*-inositol *via* regiospecific topochemical azide–alkyne cycloaddition (TAAC) polymerization.

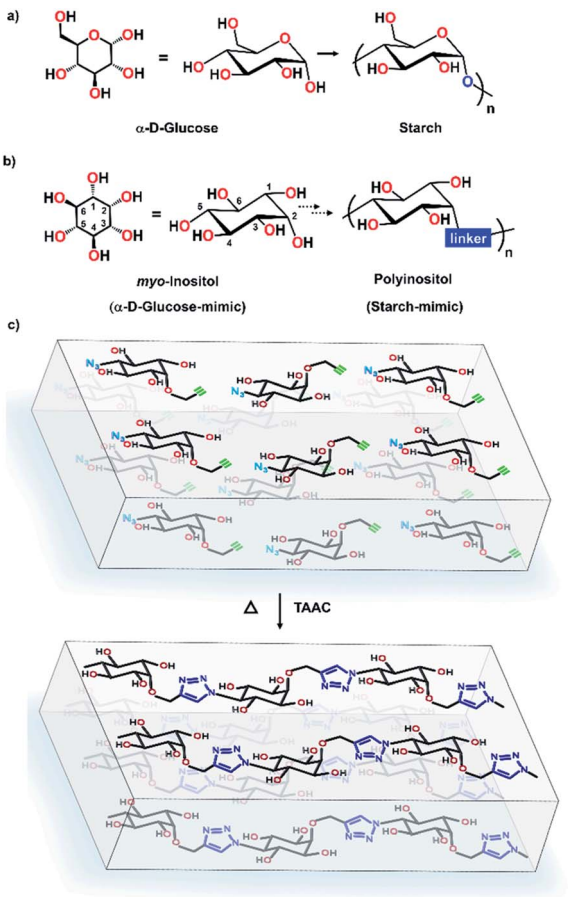

Fig. 1 (a and b) Structural similarities of α-D-glucose and *myo*-inositol & starch and polyinositol. (c) Schematic representation of SCSC synthesis of polyinositol.

School of Chemistry, Indian Institute of Science Education and Research Thiruvananthapuram, Vithura-695551, India. E-mail: kms@iisertvm.ac.in; Web: http://kms514.wix.com/kmsgroup

† Electronic supplementary information (ESI) available. CCDC 2038869 and 2038870. For ESI and crystallographic data in CIF or other electronic format see DOI: 10.1039/d1sc03727g

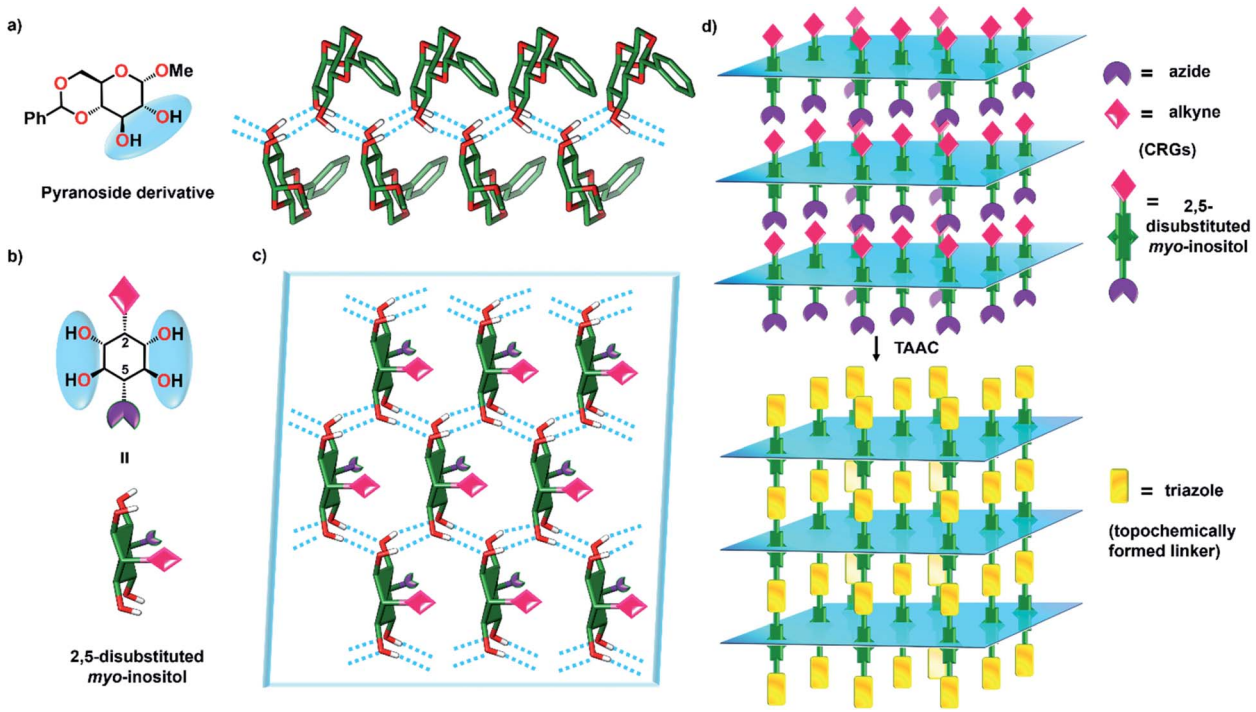

Fig. 2 (a) 1D hydrogen-bonded zigzag arrangement in crystal structures of a representative pyranoside derivative possessing diequatorial vicinal diol. (b) *myo*-Inositol derivative decorated with CRGs at 2- and 5-positions. (c) Expected 2D hydrogen-bonded layer in the *myo*-inositol derivative. (d) Proposed head-to-tail arrangement of *myo*-inositol derivatives having CRGs at 2- & 5-positions and their topochemical polymerization reaction.

Results and discussion

Design and synthesis of monomer 1

Topochemical polymerization, lattice-controlled polymerization reactions driven by proximally placed reactive groups of monomers in the crystal, offers a solvent-free and catalyst-free method for making homogeneous, stereoregular crystalline polymers in high yield.[8,9] The main challenge in the area of topochemical reactions lies in the engineering of the crystal packing to position the reacting groups at proximity in an orientation suitable for their reaction.[10] Cyclohexane/pyranoside derivatives having vicinal anti-diol consisting of two equatorial hydroxy groups consistently arrange in a zigzag fashion forming hydrogen-bonded 1D-chains, in their crystals (Fig. 2a, ESI, Section 2†).[11] We envisioned that strategically functionalizing the 2- and 5- positions of *myo*-inositol with complementary reactive groups (CRGs) *viz*. azide and alkyne, would yield tetrol **1** having two such vicinal diol units on opposite sides (Fig. 2b). This tetrol would crystallize to form a two-dimensional hydrogen-bonded layered network and stacking of such layers along the third dimension would place the azide and alkyne from adjacent layers at proximity (Fig. 2c and d). Such an arrangement would facilitate TAAC polymerization, along the direction perpendicular to the hydrogen-bonded 2D-layer, to form triazole-linked polyinositol (Fig. 2d).

To test this hypothesis, we have synthesized tetrol **1** (Scheme 1, ESI, Section 3†). Briefly, *myo*-inositol (**3**) was protected to yield the symmetric ditriflate **5**, which on selective sequential nucleophilysis with azide followed by DMSO resulted in azido-*myo*-inositol derivative **7**.[12] Propargylation of the remaining –OH group, followed by acidic hydrolysis

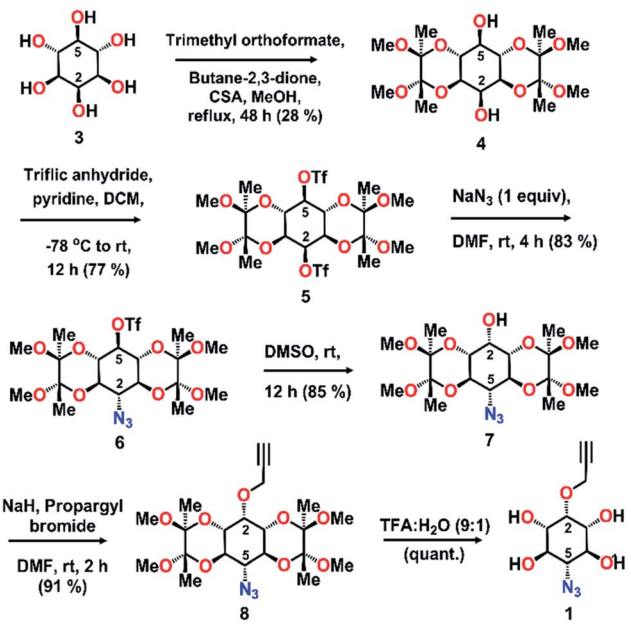

Scheme 1 Synthesis of tetrol **1**.

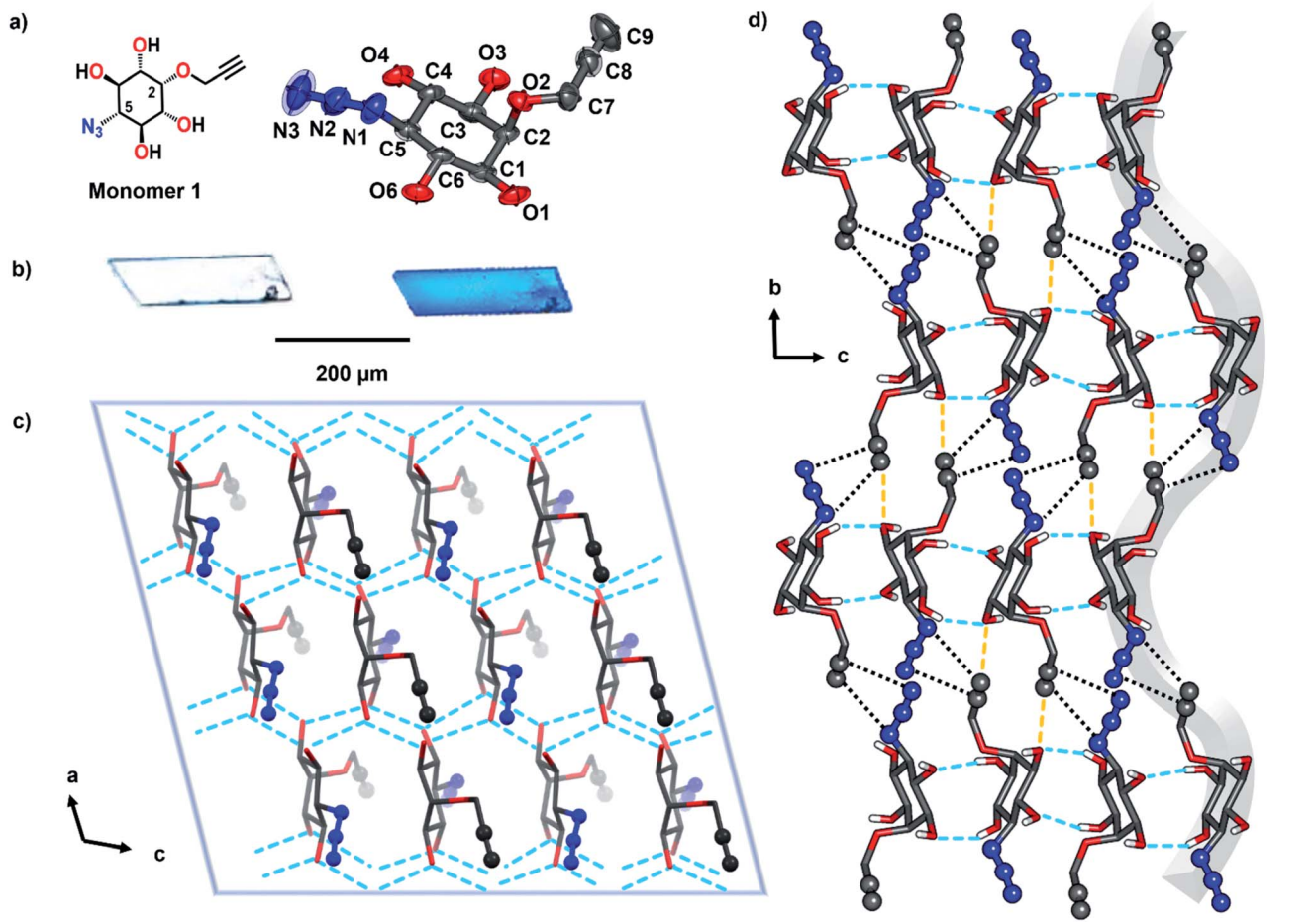

Fig. 3 (a) Chemical structure and ORTEP diagram of tetrol **1**. The thermal ellipsoids are set at 50% probability. (b) Photograph of the tetrol **1** single crystal taken under normal light and a polarizer. (c) Crystal packing of the tetrol **1** in *'ac'* plane showing a 2D hydrogen-bonded layer. (d) Crystal packing viewed along *'a'* direction. The OH···O hydrogen bonds and the CH···O hydrogen bonds are shown as blue and orange dotted lines, respectively. Black dotted lines represent the short contacts between the reactive terminals of antiparallelly arranged azide and alkyne units. The direction of polymer chain growth is along the wavy line (along *'b'* direction) shown in the background. H-atoms (except OH) are hidden for clarity.

yielded tetrol **1** as a white solid. We obtained the plate-like crystals (mp 317 °C) of tetrol **1** *via* slow evaporation of its saturated solution in acetonitrile.

Single-crystal X-ray diffraction (SCXRD) analysis revealed that the tetrol **1** crystallizes in $P2_1/n$ space group with one molecule in the asymmetric unit (Fig. 3a and Table S1†). In the crystal, the inositol ring adopts the chair conformation. The hydroxyl groups of each vicinal diol motif make intermolecular hydrogen bonding forming a hydrogen-bonded 2D-layer in the '*ac*' plane, as anticipated (Fig. 3c). Such layers stack along '*b*' direction and molecules in adjacent layers connect through CH···O hydrogen bonds (C9H9···O3, Table S2†). This stacked packing places the azide and alkyne groups of molecules in adjacent layers at proximity (3.37–3.43 Å) in a ready-to-react antiparallel arrangement (Fig. 3d).[13] The antiparallel arrangement suggests the possibility of forming 1,4-triazolyl linked polyinositol along the stacking direction.

SCSC polymerization of monomer 1

Crystals of tetrol **1** are stable at room temperature but undergo reaction at higher temperatures (80 °C and above). We have monitored the progress of the solid-state reaction using time-dependent ^{1}H NMR spectroscopy. For this, we kept crystals of the monomer **1** at 80 °C and small portions were withdrawn at various time intervals and subsequently analyzed by ^{1}H NMR (ESI, Section 5†). By the time-dependent ^{1}H NMR spectral analysis, the start of the reaction was assessed from the appearance of triazolyl proton signals in the region 7.8–8.0 ppm. With the progress of time, a gradual decrease in intensity of peaks corresponding to the monomer and the

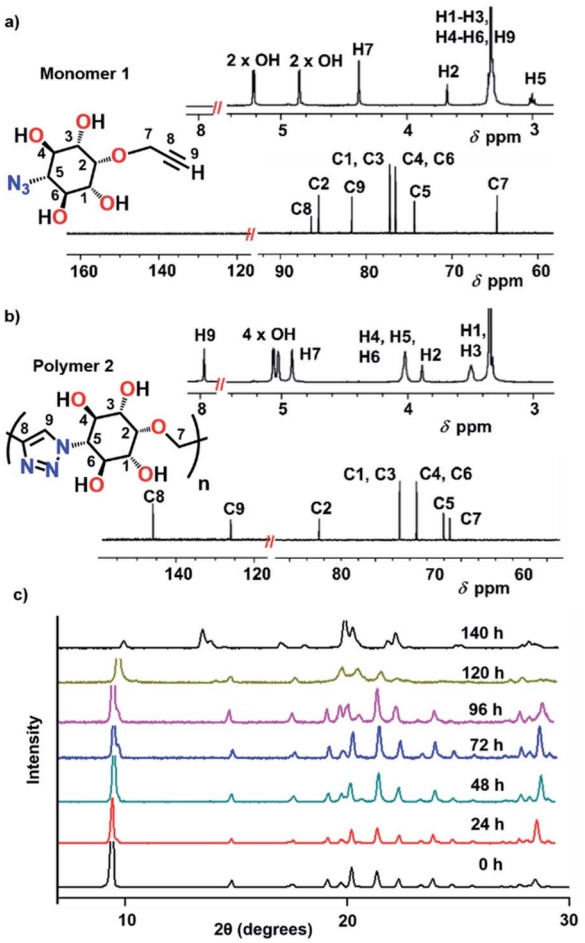

Fig. 4 ^{1}H NMR and ^{13}C NMR spectra of (a) monomer **1** and (b) polymer **2** recorded in DMSO-d_6. (c) Time-dependent PXRD analyses of monomer **1** heated at 80 °C.

concomitant increase in the intensity of peaks corresponding to the product were observed (Fig. S2†). By 140 h, the monomer was completely consumed and a single sharp triazolyl proton signal at 7.96 ppm revealed the regiospecificity of the reaction. The ^{1}H NMR and ^{13}C NMR spectra of the polymer **2** were very clear, with distinct signals for each proton and carbon atom of the repeating unit, due to the linkage-homogeneity (Fig. 4). Structural analysis using various NMR techniques revealed the presence of only 1,4-triazolyl linkages between the inositol units (ESI, Section 6†). Such a regiospecificity in this uncatalyzed solid-state reaction is possible only under strict lattice-control. It is to be noted that the uncatalyzed thermal cycloaddition reaction (Huisgen reaction) in solution proceeds without any selectivity and leads to the formation of a heterogeneous mixture of products (ESI, Section 7†), but Cu(I)-catalyzed (click) reaction in solution yields a mixture of 1,4-triazolyl-linked cyclic oligomers. The solid-state reaction followed a sigmoidal kinetics with a lag phase (0–48 h), followed by an exponential growth phase (48–120 h) and a plateau phase (Fig. S2†).

We have monitored the crystallinity throughout the reaction by recording PXRD profiles of the crystals withdrawn at different stages of reaction. Sharp signals were observed at every stage of the reaction suggesting that the crystallinity is maintained throughout the reaction. The peaks corresponding to the monomer crystal gradually disappeared or shifted and new sharp signals appeared with time (Fig. 4c). From the time-dependent PXRD data, it is clear that the monomer gradually converts to the polymer **2** in a crystal-to-crystal fashion. The morphology of the smaller crystals (length ~ 200 μm) was unaffected even after the complete reaction. Optical polarizing microscopy of the fully reacted crystals showed a birefringence pattern suggestive of its single crystalline nature (Fig. 5b). Though rare, such reactions that occur in a SCSC manner allow structure determination of the product by SCXRD.[14]

Structure and properties of polymer 2

We determined the crystal structure of the fully reacted crystals by SCXRD analysis (monoclinic $P2_1/c$ with $Z = 4$). As anticipated, TAAC reaction occurred regiospecifically in SCSC fashion and resulted in the formation of 1,4-triazolyl linked polymer **2** exclusively (Fig. 5 and Table S1†). Also, the TAAC reaction occurred along '*b*' direction connecting the hydrogen-bonded layers (Fig. 5c). In the crystal, each polymer chain adopts a wavy conformation and the adjacent inositol units are cork-screwed 180° as in the case of natural polysaccharides (Fig. 5d). Intramolecular OH···N hydrogen bonding between the triazole linker and two inositol units on its either side stabilize this conformation (Fig. 5d). This is similar to the intra-chain hydrogen bonding between the adjacent monomers in natural polysaccharides.[15] All the four hydroxyl groups in the repeating unit are involved in intermolecular (inter-chain) hydrogen bonding. Each polymer chain makes OH···O hydrogen bonding with four neighbouring chains along '*a*' direction and weak CH···N hydrogen bonds with two other neighbouring molecules along '*c*' direction (Fig. 5e). For the polymerization to occur, it is necessary that both the azide and alkyne moieties move closer.

A comparison of the arrangement of molecules in the monomer and polymer crystal structures reveals that upon polymerization, the distance between the adjacent monomer units decreased by almost 1 Å (Fig. S8 and S9†). This molecular motion results in a change in unit-cell dimensions of the polymer from that of the monomer. Since the reaction occurs along the '*b*' direction, the unit cell parameter '*b*' decreases by 9.2% and the parameters '*a*' and '*c*' increase by 2.1% and 6.7% respectively, resulting in an overall decrease in the volume of the unit cell by 3.1% (Table S1 and Fig. S8†).

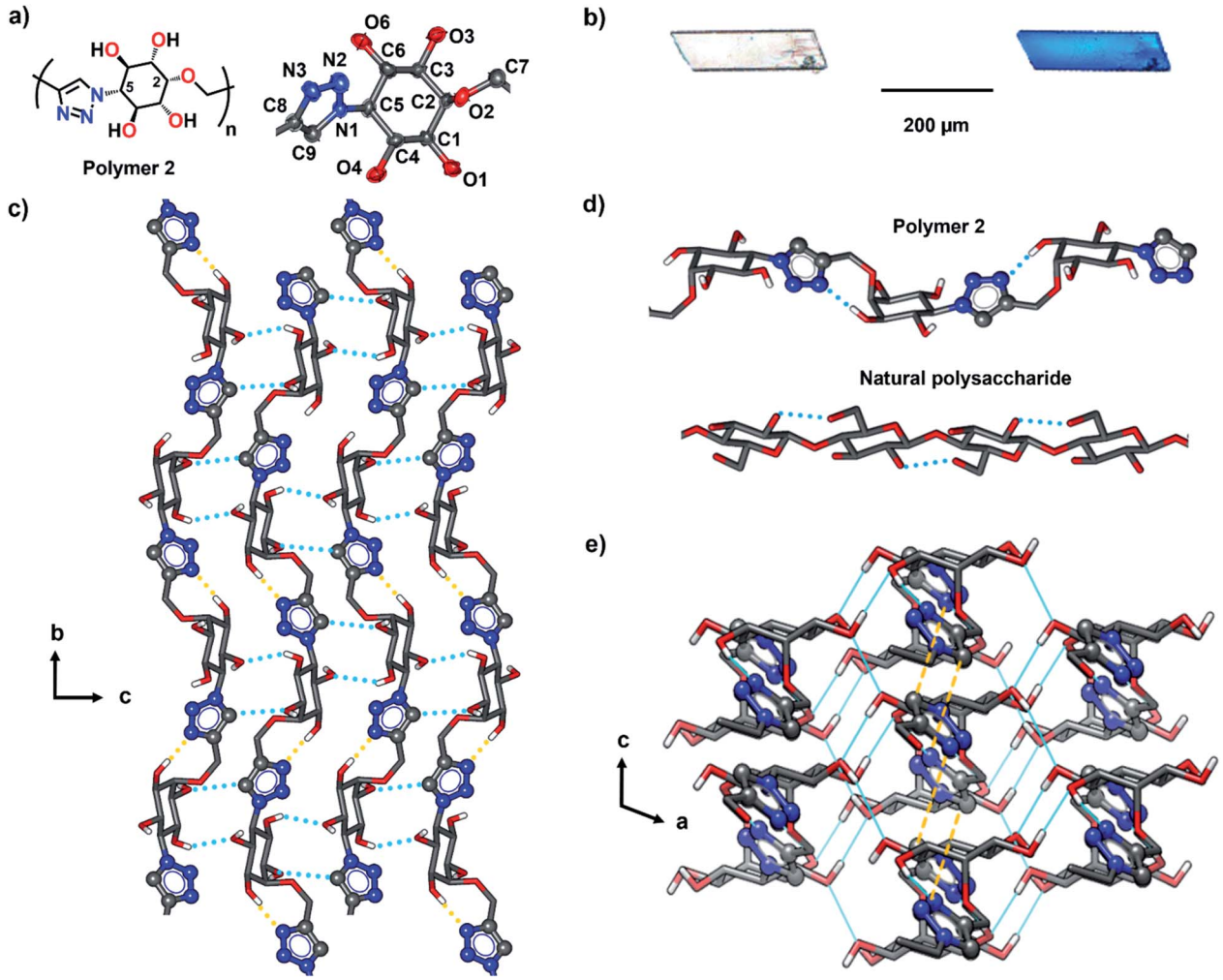

Fig. 5 (a) Chemical structure and ORTEP diagram of the polymer **2**. The thermal ellipsoids are set at 50% probability. (b) Photograph of the polymer single crystal taken under normal light and a polarizer. (c) Packing of polymer chains in '*bc*' plane showing reaction between the hydrogen-bonded layers (along '*b*' direction). The blue dotted lines represent OH···O and CH···O hydrogen bonds and the yellow dotted lines represent intra-chain OH···N hydrogen bonds. (d) Comparison of the chain conformations of polymer **2** and a natural polysaccharide. The intrachain hydrogen bonds are represented in blue lines. (e) Packing of polymer chains viewed along '*b*' direction, showing interchain hydrogen bonds. The triazole ring is represented in a ball-and-stick model and the H atoms (except OH) are hidden for clarity.

The polymer **2** crystals are soluble in DMSO and *N*-methylpyrrolidone. A MALDI-TOF MS analysis of the polymer **2** was carried out, which showed presence of up to 43-*mer* of the polyinositol (Fig. 6a). We also found that oligomers up to 8-*mer* are soluble in water (ESI, Section 9†). Gel permeation chromatography (GPC) analysis of the fully reacted sample revealed a unimodal distribution (dispersity, $Đ \sim 3$), a number-average molar mass of 4.9 kg mol^{-1} and the weight-average molar mass was calculated as 14.2 kg mol^{-1} (Fig. 6b, ESI, Section 10†). Evaporation of a DMSO solution of the polymer yields opaque polymer with a film-like texture (Fig. 6c, ESI, Section 11†). PXRD analysis of the film revealed its amorphous nature (Fig. 6d). We investigated the thermal stabilities of both the crystalline and amorphous forms of the polymer **2** using thermogravimetric analysis (TGA). While the crystals of the polymer are stable up to 344 °C, the amorphous polymer decomposed at a lower temperature of 312 °C (Fig. 6e). Thus, it is clear that the crystalline polymer shows higher thermal stability than its amorphous form. The close and ordered packing due to hydrogen bonds is responsible for the enhanced thermal stability of the crystalline polymer. Also, the crystalline polymer **2** showed better thermal stability than many natural polysaccharides.[16]

Differential scanning calorimetry (DSC) analysis of the crystalline polymer **2** did not show any glass transition (Fig. 6f) as anticipated in view of its crystalline nature, similar to crystalline amylose.[17] In contrast, the amorphous polymer **2** undergoes a glass transition at 202 °C, comparable to gelatinized starch.[18] Polymers with such high-glass transition temperatures are important in the context of stable plastics required for several applications.[19]

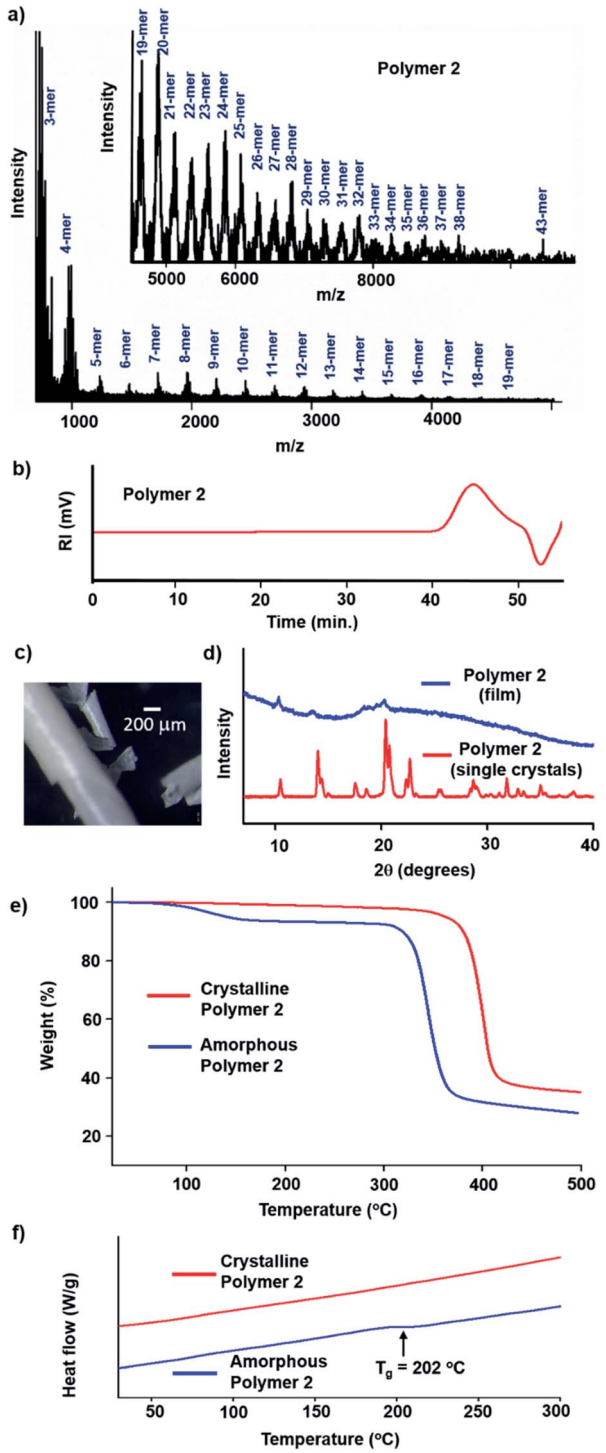

Fig. 6 (a) MALDI spectrum and (b) GPC elution curve for the polymer **2**. (c) Photograph of the polymer **2** film. (d) Comparison of PXRD patterns of polymer **2** single crystals and polymer **2** film. Comparison of (e) TGA thermograms and (f) DSC thermograms of crystalline and amorphous polymer **2** (heating rate: 5 °C min^{-1}).

Conclusions

In conclusion, circumventing the problems associated with the conventional solution-phase polymer synthesis, we have adopted a solid-state synthesis for the polymerization of a cyclitol-derived monomer. By applying crystal-engineering principles and taking a cue from the unique packing of a class of pyranose derivatives, we designed a cyclitol monomer that crystallizes such that its molecules arrange in head-to-tail fashion with the proximal placement of the azide and alkyne units of adjacent molecules. Upon heating these crystals, the monomer undergoes SCSC TAAC polymerization, in a regiospecific manner, to yield an enzyme-stable, crystalline pseudopolysaccharide, poly-1,4-triazolyl-*myo*-inositol. Despite solvent-free and catalyst-free conditions, due to the confinement offered by the crystal lattice, the reaction was not only regiospecific but also yielded linear polymer. This polycarbasugar shares key characteristics of natural polysaccharides, including the preservation of stereochemistry, dense hydroxyl functionality, and rigid backbone, in addition to being enzyme-stable, possessing higher thermal stability and higher glass transition temperature, making it a better candidate for many applications. This is the first successful synthesis of a polymer of a cyclitol using topochemical polymerization. This report exemplifies the fidelity of crystal engineering in designing topochemical reactions in general and in the synthesis of crystalline polymers. Given the availability of many structurally diverse carbasugars such as nine inositols,[3] conduritols, quercitols, other numerous naturally occurring cyclitols,[20] the possibility of extension of TAAC polymerization approach to make structurally and functionally diverse pseudopolysaccharides is huge.

Data availability

Crystallographic data for monomer **1** and polymer **2** have been deposited at the CCDC under accession numbers 2038869 and 2038870, respectively.†

Author contributions

KMS conceived the idea and designed the project. AR and AS performed the experiments. AR and KMS analysed the results and wrote the manuscript.

Conflicts of interest

There are no conflicts to declare.

Acknowledgements

KMS thanks the Department of Science and Technology, Govt. of India for a SwarnaJayanti Fellowship (DST/SJF/CSA02/2012-13) & Science and Engineering Research Board for a research grant (SERB/CRG/000577/2018).

References

1 (*a*) J. A. Galbis, M. d. G. García-Martín, M. V. de Paz and E. Galbis, *Chem. Rev.*, 2016, **116**, 1600–1636; (*b*) R. Xiao and M. W. Grinstaff, *Prog. Polym. Sci.*, 2017, **74**, 78–116; (*c*) Y. Yu and M. Delbianco, in *Recent Trends in Carbohydrate*

Chemistry, ed. A. P. Rauter, B. E. Christensen, L. Somsák, P. Kosma and R. Adamo, Elsevier, 2020, ch. 9, pp. 333–371.

2 (*a*) M. Metzke, J. Z. Bai and Z. Guan, *J. Am. Chem. Soc.*, 2003, **125**, 7760–7761; (*b*) E. L. Dane and M. W. Grinstaff, *J. Am. Chem. Soc.*, 2012, **134**, 16255–16264; (*c*) K. Mikami, A. T. Lonnecker, T. P. Gustafson, N. F. Zinnel, P.-J. Pai, D. H. Russell and K. L. Wooley, *J. Am. Chem. Soc.*, 2013, **135**, 6826–6829; (*d*) A. S. Balijepalli and M. W. Grinstaff, *Acc. Chem. Res.*, 2020, **53**, 2167–2179; (*e*) T. M. McGuire, J. Bowles, E. Deane, E. H. E. Farrar, M. N. Grayson and A. Buchard, *Angew. Chem., Int. Ed.*, 2021, **60**, 4524–4528.

3 M. P. Thomas, S. J. Mills and B. V. L. Potter, *Angew. Chem., Int. Ed.*, 2016, **55**, 1614–1650.

4 (*a*) P. Wessig and K. Möllnitz, *J. Org. Chem.*, 2012, **77**, 3907–3920; (*b*) T. Shimokawaji and A. Sudo, *J. Polym. Sci. Part A: Polym. Chem.*, 2020, **58**, 1229–1235.

5 (*a*) J.-F. Lutz, *Angew. Chem., Int. Ed.*, 2007, **46**, 1018–1025; (*b*) A. Qin, J. W. Y. Lam and B. Z. Tang, *Chem. Soc. Rev.*, 2010, **39**, 2522–2544; (*c*) J. K. Fink, in *High Performance Polymers*, ed. J. K. Fink, William Andrew Publishing, 2nd edn, 2014, ch. 9, pp. 221–240.

6 C. J. Pickens, S. N. Johnson, M. M. Pressnall, M. A. Leon and C. J. Berkland, *Bioconjug. Chem.*, 2018, **29**, 686–701.

7 (*a*) K. D. Bodine, D. Y. Gin and M. S. Gin, *J. Am. Chem. Soc.*, 2004, **126**, 1638–1639; (*b*) M. V. Rivas, G. Petroselli, R. Erra-Balsells, O. Varela and A. A. Kolender, *RSC Adv.*, 2019, **9**, 9860–9869.

8 (*a*) K. Hema, A. Ravi, C. Raju, J. R. Pathan, R. Rai and K. M. Sureshan, *Chem. Soc. Rev.*, 2021, **50**, 4062–4099; (*b*) L. Zhu, H. Tran, F. L. Beyer, S. D. Walck, X. Li, H. Ågren, K. L. Killops and L. M. Campos, *J. Am. Chem. Soc.*, 2014, **136**, 13381–13387; (*c*) Y. L. Li, C.-T. Zee, J. B. Lin, V. M. Basile, M. Muni, M. D. Flores, J. Munárriz, R. B. Kaner, A. N. Alexandrova, K. N. Houk, S. H. Tolbert and Y. Rubin, *J. Am. Chem. Soc.*, 2020, **142**, 18093–18102; (*d*) I. Levesque, J. R. Néabo, S. Rondeau-Gagné, C. Vigier-Carrière, M. Daigle and J.-F. Morin, *Chem. Sci.*, 2014, **5**, 831–836.

9 (*a*) A. Sun, J. W. Lauher and N. S. Goroff, *Science*, 2006, **312**, 1030; (*b*) T. Itoh, T. Suzuki, T. Uno, M. Kubo, N. Tohnai and M. Miyata, *Angew. Chem., Int. Ed.*, 2011, **50**, 2253–2256; (*c*) T.-J. Hsu, F. W. Fowler and J. W. Lauher, *J. Am. Chem. Soc.*, 2012, **134**, 142–145; (*d*) A. Pathigoolla, R. G. Gonnade and K. M. Sureshan, *Angew. Chem., Int. Ed.*, 2012, **51**, 4362–4366; (*e*) L. Dou, Y. Zheng, X. Shen, G. Wu, K. Fields, W.-C. Hsu, H. Zhou, Y. Yang and F. Wudl, *Science*, 2014, **343**, 272–277; (*f*) R. Z. Lange, G. Hofer, T. Weber and A. D. Schlüter, *J. Am. Chem. Soc.*, 2017, **139**, 2053–2059; (*g*) X. Jiang, X. Cui, A. J. E. Duncan, L. Li, R. P. Hughes, R. J. Staples, E. V. Alexandrov, D. M. Proserpio, Y. Wu and C. Ke, *J. Am. Chem. Soc.*, 2019, **141**, 10915–10923; (*h*) Q.-H. Guo, M. Jia, Z. Liu, Y. Qiu, H. Chen, D. Shen, X. Zhang, Q. Tu, M. R. Ryder, H. Chen, P. Li, Y. Xu, P. Li, Z. Chen, G. S. Shekhawat, V. P. Dravid, R. Q. Snurr, D. Philp, A. C. H. Sue, O. K. Farha, M. Rolandi and J. F. Stoddart, *J. Am. Chem. Soc.*, 2020, **142**, 6180–6187; (*i*) F. Hu, W. Hao, D. Mücke, Q. Pan, Z. Li, H. Qi and Y. Zhao, *J. Am. Chem. Soc.*, 2021, **143**, 5636–5642.

10 (*a*) S.-Y. Yang, X.-L. Deng, R.-F. Jin, P. Naumov, M. K. Panda, R.-B. Huang, L.-S. Zheng and B. K. Teo, *J. Am. Chem. Soc.*, 2014, **136**, 558–561; (*b*) K. Biradha and R. Santra, *Chem. Soc. Rev.*, 2013, **42**, 950–967; (*c*) S. Kusaka, A. Kiyose, H. Sato, Y. Hijikata, A. Hori, Y. Ma and R. Matsuda, *J. Am. Chem. Soc.*, 2019, **141**, 15742–15746; (*d*) I. E. Claassens, L. J. Barbour and D. A. Haynes, *J. Am. Chem. Soc.*, 2019, **141**, 11425–11429; (*e*) S. P. Yelgaonkar, G. Campillo-Alvarado and L. R. MacGillivray, *J. Am. Chem. Soc.*, 2020, **142**, 20772–20777; (*f*) J. J. Dotson, I. Liepuoniute, J. L. Bachman, V. M. Hipwell, S. I. Khan, K. N. Houk, N. K. Garg and M. A. Garcia-Garibay, *J. Am. Chem. Soc.*, 2021, **143**, 4043–4054.

11 R. Luboradzki, O. Gronwald, M. Ikeda, S. Shinkai and D. N. Reinhoudt, *Tetrahedron*, 2000, **56**, 9595–9599.

12 A. Ravi and K. M. Sureshan, *Angew. Chem., Int. Ed.*, 2018, **57**, 9362–9366.

13 G. M. J. Schmidt, *Pure Appl. Chem.*, 1971, **27**, 647–678.

14 (*a*) U. Muller, in *Symmetry Relationships between Crystal Structures: Applications of Crystallographic Group Theory in Crystal Chemistry*, Oxford University Press, 2013, ch. 11, pp. 217–224; (*b*) A. D. Schlüter, T. Weber and G. Hofer, *Chem. Soc. Rev.*, 2020, **49**, 5140–5158.

15 Y. Nishiyama, J. Sugiyama, H. Chanzy and P. Langan, *J. Am. Chem. Soc.*, 2003, **125**, 14300–14306.

16 (*a*) S. S. Kim, S. J. Kim, Y. D. Moon and Y. M. Lee, *Polymer*, 1994, **35**, 3212–3216; (*b*) M. A. Villetti, J. S. Crespo, M. S. Soldi, A. T. N. Pires, R. Borsali and V. Soldi, *J. Therm. Anal. Calorim.*, 2002, **67**, 295–303; (*c*) H. Yang, R. Yan, H. Chen, D. H. Lee and C. Zheng, *Fuel*, 2007, **86**, 1781–1788; (*d*) X. Liu, Y. Wang, L. Yu, Z. Tong, L. Chen, H. Liu and X. Li, *Starch/Stärke*, 2013, **65**, 48–60.

17 M. Scandola, G. Ceccorulli and M. Pizzoli, *Int. J. Biol. Macromol.*, 1991, **13**, 254–260.

18 A. Mizuno, M. Mitsuiki and M. Motoki, *J. Agric. Food Chem.*, 1998, **46**, 98–103.

19 H. T. H. Nguyen, P. Qi, M. Rostagno, A. Feteha and S. A. Miller, *J. Mat. Chem. A*, 2018, **6**, 9298–9331.

20 Y. Kobayashi, in *Glycoscience: Chemistry and Chemical Biology*, ed. B. O. Fraser-Reid, K. Tatsuta and J. Thiem, Springer, Berlin, Heidelberg, 2008, pp. 1913–1997.